INTERNATIONAL JOURNAL FOR NUMERICAL METHODS IN ENGINEERING
Int. J. Numer. Meth. Engng 2010; **84**:1166–1182
Published online 17 May 2010 in Wiley Online Library (wileyonlinelibrary.com). DOI: 10.1002/nme.2935

Inverse finite element method for large-displacement beams

Alejandro E. Albanesi, Víctor D. Fachinotti*, † and Alberto Cardona

Centro Internacional de Métodos Computacionales en Ingeniería (*CIMEC-INTEC*), *Universidad Nacional del Litoral-CONICET*, *Güemes 3450*, *3000 Santa Fe*, *Argentina*

SUMMARY

A finite element model for the inverse analysis of large-displacement beams in the elastic range is presented. The model permits determining the initial shape of a beam such that it attains the given design shape under the effect of service loads. This formulation has immediate applications in various fields such as compliant mechanism design where flexible links can be modeled as large-displacement beams. Numerical tests for validation purposes are given, together with two design applications of flexible mechanisms with distributed compliance: a flexible gripper and a flexible S-type clutch. Copyright © 2010 John Wiley & Sons, Ltd.

Received 4 February 2010; Revised 7 April 2010; Accepted 11 April 2010

KEY WORDS: inverse FEM; large-displacement beams; compliant mechanisms

1. INTRODUCTION

The classical (direct) problem in Elasticity consists in computing the deformed shape of a body knowing its mechanical properties and the applied loads in a given undeformed (reference) configuration. The deformed configuration—unknown at the start of the analysis—is computed as the solution of this direct problem, which is inherently non-linear when large deformations are involved. In this work we deal with the inverse problem, i.e. to determine the undeformed (reference) configuration knowing the deformed shape of the body and the applied loads. Beck and Woodburry [1] classified it as an inverse design problem, in contrast to classical inverse (measurement) problems that consist in determining material data knowing both the deformed and undeformed configurations, as well as the service loads.

*Correspondence to: Víctor D. Fachinotti, Centro Internacional de Métodos Computacionales en Ingeniería (CIMEC-INTEC), Universidad Nacional del Litoral-CONICET, Güemes 3450, 3000 Santa Fe, Argentina.
†E-mail: vfachino@intec.unl.edu.ar

Contract/grant sponsor: Consejo Nacional de Investigaciones Científicas y Técnicas de la República Argentina (CONICET)

Inverse methods constitute a very useful tool that allows engineers to conceive designs in less time and at lower costs than those involved in traditional experimental and direct computational design. Also, the iterative trial and error approach used many times in design processes is avoided. Finite element models for the inverse design of two- and three-dimensional isotropic elastic continuum bodies subjected to large deformations have been proposed by Govindjee and co-workers [2–4] and Yamada [5]. Later, Govindjee [6] extended the inverse finite element design to hyperelastic orthotropic materials with applications to axi-symmetric problems. More recently, Lu *et al.* [7] and Fachinotti *et al.* [8] developed three-dimensional models for the inverse design of orthotropic hyperelastic solids. Also, inverse finite element was applied to the design of shells [9].

In this paper, we focused on the design of compliant mechanisms and extended our previous work [8] to two- and three-dimensional highly flexible beam structures. To this end, we formulated an inverse finite element model based on the non-linear beam formulation proposed by Cardona and Géradin [10, 11]. Compliant mechanisms necessarily have low mass and very high flexibility, so large displacements behavior ought to be considered. We proceeded by formulating the kinematic beam assumptions before expressing non-linear strain measures. We used the rotational vector to parameterize rotations, since it has a simple geometric meaning and does not introduce any singularity in representing rotations of any magnitude. We further assumed that beam cross-sections remain straight but the beam could undergo shear strains. For the purpose of flexible mechanism analysis and synthesis, a simplified linear elastic constitutive relation was adopted. Although flexibility effects were introduced using a large displacement hypothesis with finite rotations, we assumed that the strains which resulted were small.

Two simple tests were proposed for validation purposes. The first one was the two-dimensional bending of a cantilever beam, for which an analytical solution is available [12]. The second problem is the 45-degree bend of a cantilever beam, which has been widely used as a benchmark for three-dimensional flexible beams models [10, 11, 13–15].

Finally, two examples of applications in the field of compliant mechanisms analysis are shown: the design of a flexible gripper previously studied by Lan and Cheng [16], and the design of an S-type flexible clutch.

2. BEAM KINEMATICS

Let us consider a beam of cross-section $\mathscr{A}_0$ and length L, with initial configuration $\mathscr{B}_0 = \mathscr{A}_0 \times [0, L] \in R^3$ and current deformed configuration $\mathscr{B} = \mathscr{A} \times [0, l] \in R^3$ (Figure 1). We assume that deformation of the beam takes place such that the cross-section does not change and remains plane; however, shear effects make the cross-section to not remain normal to the centroidal line [10, 11].

The current position $\boldsymbol{x} \in \mathscr{B}$ of a generic point can be expressed as

$$\boldsymbol{x}(s) = \boldsymbol{x}_0(s) + \boldsymbol{y}(s)$$

where s is the length parameter along the neutral axis of the beam, $\boldsymbol{x}_0$ is the trace of the neutral axis on the cross-section $\mathscr{A}$ containing the point $\boldsymbol{x}$ and normal to the neutral axis, and $\boldsymbol{y}$ is the position of $\boldsymbol{x}$ in the cross-section relative to $\boldsymbol{x}_0$.

Before deformation, this same material point occupied the position $\boldsymbol{X} \in \mathscr{B}_0$:

$$\boldsymbol{X}(S) = \boldsymbol{X}_0(S) + \boldsymbol{Y}(S)$$

DOI: 10.1002/nme

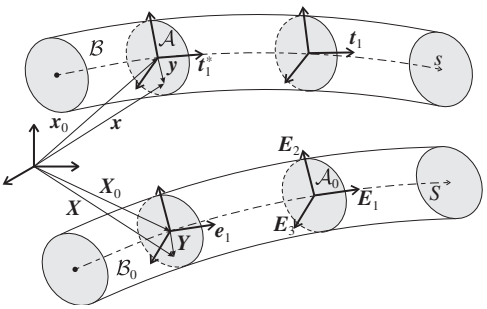

Figure 1. Description of beam kinematics.

where S is the length parameter along the neutral axis of the undeformed beam, $\boldsymbol{X}_0 \in \mathscr{B}_0$ is the position occupied by the point at $\boldsymbol{x}_0 \in \mathscr{B}$ before deformation, and $\boldsymbol{Y}$ is the position of $\boldsymbol{X}$ relative to $\boldsymbol{X}_0$.

Vectors $\boldsymbol{y}$ and $\boldsymbol{Y}$ are related by

$$\boldsymbol{Y} = \boldsymbol{R}^{\mathrm{T}} \boldsymbol{y} \tag{1}$$

where $\boldsymbol{R}$ is the so-called rotation operator, which belongs to the Lie group of proper orthogonal linear transformations. Since sections are assumed to remain plane during deformation, the transformation (1) is constant on the cross-section $\mathscr{A}$.

Let $\{\boldsymbol{E}_1, \boldsymbol{E}_2, \boldsymbol{E}_3\}$ be an orthonormal basis in $\mathscr{B}_0$, such that $\boldsymbol{E}_1 = \mathrm{d}\boldsymbol{X}_0/\mathrm{d}S$ is tangent to the neutral axis, and $\boldsymbol{E}_2$ and $\boldsymbol{E}_3$ define the principal axes of inertia of the cross-section $\mathscr{A}_0$ of the undeformed beam. The corresponding orthonormal triad in $\mathscr{B}$ is $\{\boldsymbol{t}_1, \boldsymbol{t}_2, \boldsymbol{t}_3\}$, with

$$\boldsymbol{t}_i = \boldsymbol{R}\boldsymbol{E}_i, \quad i = 1, 2, 3$$

Let us also consider an orthonormal basis $\{\boldsymbol{t}_1^*, \boldsymbol{t}_2^*, \boldsymbol{t}_3^*\}$ in $\mathscr{B}$, such that $\boldsymbol{t}_1^* = \mathrm{d}\boldsymbol{x}_0/\mathrm{d}s$ is normal to the cross-section $\mathscr{A}$ and tangent to the neutral axis, and $\boldsymbol{t}_2^*, \boldsymbol{t}_3^*$ are aligned along the directions of the principal axes of inertia of the cross-section. The corresponding orthonormal triad in $\mathscr{B}$ is $\{\boldsymbol{e}_1, \boldsymbol{e}_2, \boldsymbol{e}_3\}$, with

$$\boldsymbol{e}_i = \boldsymbol{R}^{\mathrm{T}} \boldsymbol{t}_i^*, \quad i = 1, 2, 3$$

Note that although $\boldsymbol{t}_1^*$ and $\boldsymbol{E}_1$ are aligned with the neutral axes in $\mathscr{B}$ and $\mathscr{B}_0$, respectively, $\boldsymbol{e}_1$ and $\boldsymbol{t}_1$ are not general aligned with the neutral axes in $\mathscr{B}_0$ and $\mathscr{B}$ because of shear deformation. We remark that, for the same reason, $\mathscr{A}$ and $\mathscr{A}_0$ do not contain the same material points.

In the inverse analysis, the variables $\boldsymbol{x}_0$ that determine $\mathscr{B}$ are assumed to be known. Then, we have to solve a problem for the unknowns $\boldsymbol{X}_0$ and $\boldsymbol{R}$ in order to completely determine $\mathscr{B}_0$.

2.1. Parameterization of rotations

Let us introduce the Cartesian rotational vector $\boldsymbol{\psi}$, which is defined as the vector whose direction is that of the rotation axis $\boldsymbol{n}$ and whose length is equal to the amplitude of the rotation ψ:

$$\boldsymbol{\psi} = \boldsymbol{n}\psi$$

DOI: 10.1002/nme

Using $\boldsymbol{\psi}$, the rotation operator in three-dimensional space is completely determined by means of Rodrigues formula:

$$\boldsymbol{R}(\boldsymbol{\psi})=\boldsymbol{I}+\frac{\sin\psi}{\psi}\widetilde{\boldsymbol{\psi}}+\frac{1-\cos\psi}{\psi^2}\widetilde{\boldsymbol{\psi}}\widetilde{\boldsymbol{\psi}} \tag{2}$$

where $\boldsymbol{I}$ is the identity matrix and, from now on, $\widetilde{\boldsymbol{u}}$ is the skew-symmetric matrix associated with the vector $\boldsymbol{u}$ given as

$$\widetilde{\boldsymbol{u}}=\begin{bmatrix} 0 & -u_3 & u_2 \\ u_3 & 0 & -u_1 \\ -u_2 & u_1 & 0 \end{bmatrix}$$

Using this operator, the cross product of two vectors $\boldsymbol{u}$ and $\boldsymbol{v}$ can be obtained as

$$\boldsymbol{u}\times\boldsymbol{v}=\widetilde{\boldsymbol{u}}\boldsymbol{v}$$

Let us note that $\boldsymbol{R}\to\boldsymbol{I}$ when $\psi\to 0$.

Since $\boldsymbol{\psi}$ suffices to completely describe the rotation $\boldsymbol{R}$, we consider the minimal set of variables $\{\boldsymbol{X}_0,\boldsymbol{\psi}\}$—instead of $\{\boldsymbol{X}_0,\boldsymbol{R}\}$—as unknown fields of the inverse problem.

2.2. *Spatial deformation measures*

Material deformation measures are given by the vectors of deformation of the neutral axis $\boldsymbol{\Gamma}$ and curvature $\boldsymbol{K}$ [11]:

$$\boldsymbol{\Gamma}=\boldsymbol{R}^{\mathrm{T}}\frac{\mathrm{d}\boldsymbol{x}_0}{\mathrm{d}S}-\frac{\mathrm{d}\boldsymbol{X}_0}{\mathrm{d}S}$$

$$\boldsymbol{K}=\boldsymbol{T}\frac{\mathrm{d}\boldsymbol{\psi}}{\mathrm{d}S}$$

where $\boldsymbol{T}$ is the tangent operator

$$\boldsymbol{T}(\boldsymbol{\psi})=\boldsymbol{I}+\frac{\cos\psi-1}{\psi^2}\widetilde{\boldsymbol{\psi}}+\left(1-\frac{\sin\psi}{\psi}\right)\widetilde{\boldsymbol{\psi}}\widetilde{\boldsymbol{\psi}} \tag{3}$$

(note that $\boldsymbol{T}\to\boldsymbol{I}$ as $\psi\to 0$).

The spatial counterparts of vectors $\boldsymbol{\Gamma}$ and $\boldsymbol{K}$, say $\boldsymbol{\gamma}$ and $\boldsymbol{\kappa}$, respectively, are obtained by applying a rotation to the current configuration:

$$\boldsymbol{\gamma}=\boldsymbol{R}\boldsymbol{\Gamma}=\frac{\mathrm{d}\boldsymbol{x}_0}{\mathrm{d}S}-\boldsymbol{R}\frac{\mathrm{d}\boldsymbol{X}_0}{\mathrm{d}S}$$

$$\boldsymbol{\kappa}=\boldsymbol{R}\boldsymbol{K}=\boldsymbol{R}\boldsymbol{T}\frac{\mathrm{d}\boldsymbol{\psi}}{\mathrm{d}S}$$

Since the length parameter S along the undeformed beam can be expressed as a function of the current length parameter s, the derivative of any function ϕ with respect to S can be computed

DOI: 10.1002/nme

using the chain rule:

$$\frac{\mathrm{d}\phi}{\mathrm{d}S}=\frac{\phi'}{S'}$$

with $(*)'\equiv \mathrm{d}(*)/\mathrm{d}s$. Then, the *spatial* measures of the deformation of the neutral axis and curvature, referred to the *known deformed frame*, can be computed using the expressions:

$$\boldsymbol{\gamma}=\frac{1}{S'}(\boldsymbol{x}_0'-\boldsymbol{R}\boldsymbol{X}_0') \tag{4}$$

$$\boldsymbol{\kappa}=\frac{1}{S'}\boldsymbol{R}\boldsymbol{T}\boldsymbol{\psi}' \tag{5}$$

3. GOVERNING EQUILIBRIUM EQUATIONS

We formulate the equilibrium equations in the known deformed configuration $\mathscr{B}$ [8]. Let $\mathscr{A}$ be the cross-section containing point $\boldsymbol{x}\in\mathscr{B}$ and normal to the neutral axis in the deformed configuration. The area of $\mathscr{A}$ is assumed to be constant along the beam. Let us call $\boldsymbol{n}$ and $\boldsymbol{m}$ the resultant force and moment with respect to $\boldsymbol{x}_0$ of the tractions acting over the surface $\mathscr{A}$, and $\bar{\boldsymbol{n}}$ and $\bar{\boldsymbol{m}}$ the external force and moment per unit length at $\boldsymbol{x}$.

Then, assuming static conditions, the translational and rotational equilibrium equations at every point $\boldsymbol{x}\in\mathscr{B}$ can be expressed as follows:

$$\boldsymbol{n}'+\bar{\boldsymbol{n}}=\boldsymbol{0}$$

$$\boldsymbol{m}'+\boldsymbol{x}_0'\times\boldsymbol{n}+\bar{\boldsymbol{m}}=\boldsymbol{0}$$

The weak form of the equilibrium equations over $\mathscr{B}$ can be written as:

$$\int_{\mathscr{B}}(\boldsymbol{n}'+\bar{\boldsymbol{n}})^{\mathrm{T}}\delta\boldsymbol{X}_0\,\mathrm{d}s+\int_{\mathscr{B}}(\boldsymbol{m}'+\boldsymbol{x}_0'\times\boldsymbol{n}+\bar{\boldsymbol{m}})^{\mathrm{T}}\delta\boldsymbol{\psi}\,\mathrm{d}s=0$$

where $\delta\boldsymbol{X}_0$ and $\delta\boldsymbol{\psi}$ are admissible variations of $\boldsymbol{X}_0$ and $\boldsymbol{\psi}$.

Finally, after integration by parts, the equivalent variational problem takes the following form: *Find* $\boldsymbol{X}_0(s)$ *and* $\boldsymbol{\psi}(s)$ *such that*

$$\int_{\mathscr{B}}[\boldsymbol{n}^{\mathrm{T}}(\delta\boldsymbol{X}_0'+\boldsymbol{x}_0'\times\delta\boldsymbol{\psi})+\boldsymbol{m}^{\mathrm{T}}\delta\boldsymbol{\psi}']\,\mathrm{d}s=\int_{\mathscr{B}}(\bar{\boldsymbol{n}}^{\mathrm{T}}\delta\boldsymbol{X}_0+\bar{\boldsymbol{m}}^{\mathrm{T}}\delta\boldsymbol{\psi})\,\mathrm{d}s \tag{6}$$

for all admissible $\delta\boldsymbol{X}_0$ *and* $\delta\boldsymbol{\psi}$.

3.1. Constitutive equations

Let us make the following assumptions [11]:

- the material remains in the linear elastic range, and
- although the beam may undergo large rigid-body rotations, its material strains remain small.

DOI: 10.1002/nme

Then, the following linear constitutive laws apply:

$$\boldsymbol{n} = \boldsymbol{C}^n \boldsymbol{\gamma} \tag{7}$$

$$\boldsymbol{m} = \boldsymbol{C}^m \boldsymbol{\kappa} \tag{8}$$

where $\boldsymbol{C}^n = C^n_{ij}\, \boldsymbol{t}^*_i \otimes \boldsymbol{t}^*_j$ and $\boldsymbol{C}^m = C^m_{ij}\, \boldsymbol{t}^*_i \otimes \boldsymbol{t}^*_j$ are the second-order tensors of elastic integrated properties over the cross-section. The matrices of elastic coefficients C^n_{ij} and C^m_{ij} referred to the principal axes of the deformed beam are written:

$$C^n = \begin{bmatrix} EA & 0 & 0 \\ 0 & GA_2 & 0 \\ 0 & 0 & GA_3 \end{bmatrix}, \quad C^m = \begin{bmatrix} GJ & 0 & 0 \\ 0 & EI_2 & 0 \\ 0 & 0 & EI_3 \end{bmatrix}$$

being EA the axial stiffness, GA_i the shear bending stiffness along the transverse axis $\boldsymbol{t}^*_i$, GJ the torsional stiffness, and EI_i the bending stiffness along the principal axis $\boldsymbol{t}^*_i$ $(i = 2, 3)$.

4. FINITE ELEMENT METHOD

Based on the 'direct' beam element proposed by Géradin and Cardona [11], the current 'inverse' beam element representing the deformed configuration $\mathscr{B}$ is a straight, mixed linear–linear finite element. The element geometry is linearly interpolated:

$$\boldsymbol{x}_0(s) = \varphi_1(s)\boldsymbol{x}^1_0 + \varphi_2(s)\boldsymbol{x}^2_0, \quad 0 \leqslant s \leqslant l = \|\boldsymbol{x}^2_0 - \boldsymbol{x}^1_0\|$$

where $\boldsymbol{x}^i_0$ is the position of node i, $i = 1, 2$, and φ_i is the linear shape function associated with node i, defined as (Figure 2)

$$\varphi_1 = 1 - \frac{s}{l}, \quad \varphi_2 = \frac{s}{l}$$

The unknowns of the inverse problem are approximated as follows:

$$\boldsymbol{X}_0(s) = \varphi_1(s)\boldsymbol{X}^1_0 + \varphi_2(s)\boldsymbol{X}^2_0 \tag{9}$$

$$\boldsymbol{\psi}(s) = \varphi_1(s)\boldsymbol{\psi}^1 + \varphi_2(s)\boldsymbol{\psi}^2 \tag{10}$$

where $\boldsymbol{X}^i_0$ and $\boldsymbol{\psi}^i$ are, respectively, the unknown values of $\boldsymbol{X}_0$ and $\boldsymbol{\psi}$ at node i.

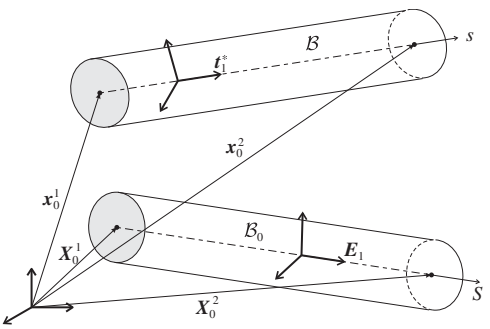

Figure 2. Finite element model of the inverse beam.

DOI: 10.1002/nme

Since $\boldsymbol{x}_0$ and $\boldsymbol{X}_0$ are both linearly interpolated, arc-length parameters s and S along the neutral axes in the deformed and undeformed configurations are related by the linear expression:

$$S = \frac{L}{l} s$$

with $L = \|\boldsymbol{X}_0^2 - \boldsymbol{X}_0^1\|$, and then

$$S' = \frac{L}{l}$$

4.1. Discretized equilibrium equations

Following the standard Galerkin finite element formulation [17], we approximate the unknowns $\boldsymbol{X}_0$ and $\boldsymbol{\psi}$ as well as their variations using Equations (9) and (10). Then, the equilibrium equations (6) give rise to the following non-linear system of algebraic equations for the nodal unknowns $\boldsymbol{X}_0^i$ and $\boldsymbol{\psi}^i$:

$$\boldsymbol{F}_{\text{int}}(\boldsymbol{Q}) - \boldsymbol{F}_{\text{ext}} = \boldsymbol{0} \tag{11}$$

where $\boldsymbol{Q}$ is the vector of nodal unknowns defined as

$$\boldsymbol{Q} = \begin{bmatrix} \boldsymbol{X}_0^1 \\ \boldsymbol{\psi}^1 \\ \boldsymbol{X}_0^2 \\ \boldsymbol{\psi}^2 \end{bmatrix}$$

and where $\boldsymbol{F}_{\text{int}}$ and $\boldsymbol{F}_{\text{ext}}$ are the vectors of internal and external forces, respectively, given by

$$\boldsymbol{F}_{\text{int}} = \int_{\mathscr{B}} \boldsymbol{B}^{\mathrm{T}} \boldsymbol{\sigma} \, \mathrm{d}s, \quad \boldsymbol{F}_{\text{ext}} = \int_{\mathscr{B}} \boldsymbol{\varphi}^{\mathrm{T}} \bar{\boldsymbol{t}} \, \mathrm{d}s$$

with

$$\boldsymbol{B} = \begin{bmatrix} \varphi_1' \boldsymbol{I} & \varphi_1 \widetilde{\boldsymbol{x}_0'} & \varphi_2' \boldsymbol{I} & \varphi_2 \widetilde{\boldsymbol{x}_0'} \\ \boldsymbol{O} & \varphi_1' \boldsymbol{I} & \boldsymbol{O} & \varphi_2' \boldsymbol{I} \end{bmatrix}, \quad \boldsymbol{\sigma} = \begin{bmatrix} \boldsymbol{n} \\ \boldsymbol{m} \end{bmatrix}$$

$$\boldsymbol{\varphi} = \begin{bmatrix} \varphi_1 \boldsymbol{I} & \boldsymbol{O} & \varphi_2 \boldsymbol{I} & \boldsymbol{O} \\ \boldsymbol{O} & \varphi_1 \boldsymbol{I} & \boldsymbol{O} & \varphi_2 \boldsymbol{I} \end{bmatrix}, \quad \bar{\boldsymbol{t}} = \begin{bmatrix} \bar{\boldsymbol{n}} \\ \bar{\boldsymbol{m}} \end{bmatrix}$$

Here, $\boldsymbol{O}$ is the 3×3 null matrix and $\boldsymbol{I}$ is the 3×3 identity matrix; note also that $\varphi_1' = -1/l$, $\varphi_2' = 1/l$ and $\boldsymbol{x}_0' = (\boldsymbol{x}_0^2 - \boldsymbol{x}_0^1)/l$ are constant within the element.

The external loads $\bar{\boldsymbol{n}}$ and $\bar{\boldsymbol{m}}$ are assumed to be given and independent of the unknowns; therefore the external force vector $\boldsymbol{F}_{\text{ext}}$ does not depend on the unknowns.

The internal force vector $\boldsymbol{F}_{\text{int}}$ depends on the unknowns via the internal efforts $\boldsymbol{\sigma}$, whose dependence on the unknowns will be analyzed in next section.

DOI: 10.1002/nme

In order to avoid shear locking, $\boldsymbol{F}_{\text{int}}$ is evaluated using reduced integration with only one sampling point located at $s=l/2$, yielding:

$$\boldsymbol{F}_{\text{int}}=\boldsymbol{B}_{sp}^{\text{T}}\boldsymbol{\sigma}_{sp}\,l$$

where $(*)_{sp}\equiv *|_{s=l/2}$, and

$$\boldsymbol{B}_{sp}=\frac{1}{l}\begin{bmatrix}-\boldsymbol{I} & \frac{1}{2}\widetilde{\Delta\boldsymbol{x}_0} & \boldsymbol{I} & \frac{1}{2}\widetilde{\Delta\boldsymbol{x}_0}\\ \boldsymbol{O} & -\boldsymbol{I} & \boldsymbol{O} & \boldsymbol{I}\end{bmatrix}$$

with $\Delta\boldsymbol{x}_0=\boldsymbol{x}_0^2-\boldsymbol{x}_0^1$.

4.2. Computation of deformation and stress in the current finite element

By evaluating Equations (4) and (5) at the sampling point, we obtain:

$$\boldsymbol{\gamma}_{sp}=\frac{1}{L}(\Delta\boldsymbol{x}_0-\boldsymbol{R}_{sp}\Delta\boldsymbol{X}_0) \tag{12}$$

$$\boldsymbol{\kappa}_{sp}=\frac{1}{L}\boldsymbol{R}_{sp}\boldsymbol{T}_{sp}\Delta\boldsymbol{\psi} \tag{13}$$

with $\Delta\boldsymbol{X}_0=\boldsymbol{X}_0^2-\boldsymbol{X}_0^1$, $\Delta\boldsymbol{\psi}=\boldsymbol{\psi}^2-\boldsymbol{\psi}^1$, and $\boldsymbol{R}_{sp}=\boldsymbol{R}(\boldsymbol{\psi}_{sp})$ and $\boldsymbol{T}_{sp}=\boldsymbol{T}(\boldsymbol{\psi}_{sp})$ are given by Equations (2) and (3), respectively, evaluated at $\boldsymbol{\psi}_{sp}=(\boldsymbol{\psi}^1+\boldsymbol{\psi}^2)/2$.

Now, the internal efforts at the sampling point are obtained using Equations (7) and (8):

$$\boldsymbol{n}_{sp}=\boldsymbol{C}^n\boldsymbol{\gamma}_{sp}$$

$$\boldsymbol{m}_{sp}=\boldsymbol{C}^m\boldsymbol{\kappa}_{sp}$$

4.3. Linearization of the discrete equilibrium equations

The non-linear discrete equilibrium equations (11) are solved using the Newton–Raphson method [17]. At each iteration k, the residual vector $\boldsymbol{F}=\boldsymbol{F}_{\text{int}}-\boldsymbol{F}_{\text{ext}}$ is approximated using the linear Taylor expansion:

$$\boldsymbol{F}^{(k)}\approx\boldsymbol{F}^{(k-1)}+\boldsymbol{S}^{(k-1)}(\boldsymbol{Q}^{(k)}-\boldsymbol{Q}^{(k-1)})=\boldsymbol{0}$$

where $\boldsymbol{S}^{(k-1)}$ is the tangent stiffness matrix:

$$\boldsymbol{S}=\frac{\mathrm{d}\boldsymbol{F}}{\mathrm{d}\boldsymbol{Q}}$$

evaluated at iteration $(k-1)$.

As already mentioned, only the internal forces are assumed to depend on the unknowns. By differentiating $\boldsymbol{F}_{\text{int}}$ with respect to the unknowns $\boldsymbol{Q}$, we obtain

$$\boldsymbol{S}=l\boldsymbol{B}_{sp}^{\text{T}}\frac{\mathrm{d}\boldsymbol{\sigma}_{sp}}{\mathrm{d}\boldsymbol{Q}}$$

DOI: 10.1002/nme

Then, it only remains to compute the derivatives of the stresses, evaluated at the sampling point $s=l/2$, with respect to $\boldsymbol{Q}$:

$$\frac{\mathrm{d}\boldsymbol{\sigma}_{sp}}{\mathrm{d}\boldsymbol{Q}}=\begin{bmatrix}\dfrac{\mathrm{d}\boldsymbol{n}_{sp}}{\mathrm{d}\boldsymbol{Q}}\\[2ex]\dfrac{\mathrm{d}\boldsymbol{m}_{sp}}{\mathrm{d}\boldsymbol{Q}}\end{bmatrix}=\begin{bmatrix}\boldsymbol{C}^n & \boldsymbol{O}\\ \boldsymbol{O} & \boldsymbol{C}^m\end{bmatrix}\begin{bmatrix}\dfrac{\mathrm{d}\boldsymbol{\gamma}_{sp}}{\mathrm{d}\boldsymbol{X}_0^1} & \dfrac{\mathrm{d}\boldsymbol{\gamma}_{sp}}{\mathrm{d}\boldsymbol{\psi}^1} & \dfrac{\mathrm{d}\boldsymbol{\gamma}_{sp}}{\mathrm{d}\boldsymbol{X}_0^2} & \dfrac{\mathrm{d}\boldsymbol{\gamma}_{sp}}{\mathrm{d}\boldsymbol{\psi}^2}\\[2ex]\dfrac{\mathrm{d}\boldsymbol{\kappa}_{sp}}{\mathrm{d}\boldsymbol{X}_0^1} & \dfrac{\mathrm{d}\boldsymbol{\kappa}_{sp}}{\mathrm{d}\boldsymbol{\psi}^1} & \dfrac{\mathrm{d}\boldsymbol{\kappa}_{sp}}{\mathrm{d}\boldsymbol{X}_0^2} & \dfrac{\mathrm{d}\boldsymbol{\kappa}_{sp}}{\mathrm{d}\boldsymbol{\psi}^2}\end{bmatrix}$$

The detailed computation of the derivatives of the deformation measures is given in the Appendix.

5. VALIDATION EXAMPLES

5.1. Bending of a flexible cantilever beam

Let us consider the plane bending of a flexible cantilever beam with constant rectangular cross-section, whose geometrical and material properties are listed in Table I. We assume the beam is clamped at the origin of a reference frame O-xyz, and it is aligned along the x-axis in the undeformed configuration. It bends in the xz plane under a force $P=10^5$ N exerted at the free end in the z-direction. The magnitude of force is such that the resulting deflections are large, out of the range of linearized beam deflection equations.

In order to define the domain of inverse analysis, we need to know the whole elastica. An analytical expression of the elastica can be computed by assuming that shear effects on deformation are negligible. This hypothesis is well justified since the beam has a high slenderness ratio. The large deflection $w(x)$ of a cantilever beam with bending stiffness EI_y under a vertical load P applied at the free end is given by the solution of the differential equation:

$$\frac{\mathrm{d}^2w}{\mathrm{d}x^2}+\frac{P}{EI}(x_{\mathrm{tip}}-x)\left(1+\frac{\mathrm{d}w}{\mathrm{d}x}\right)^{3/2}=0$$

subject to the boundary conditions:

$$w(0)=0,\qquad \left.\frac{\mathrm{d}w}{\mathrm{d}x}\right|_{x=0}=0$$

Table I. Geometrical and material data for the problem of plane bending of a flexible cantilever beam.

Beam width	$b=3\,\mathrm{cm}$
Beam height	$d=6\,\mathrm{cm}$
Beam length	$L=2\,\mathrm{m}$
Young's modulus	$E=2.10\times10^{11}\,\mathrm{N/m^2}$
Shear modulus	$G=1.05\times10^{11}\,\mathrm{N/m^2}$

DOI: 10.1002/nme

The solution of the above boundary value problem is

$$w(x)=\int_0^x \frac{1}{\sqrt{\beta^2(\chi)-1}}\,\mathrm{d}\chi, \quad 0\leqslant x\leqslant x_{\mathrm{tip}} \tag{14}$$

with

$$\beta(\chi)=\left[\frac{P}{EI}\left(x_{\mathrm{tip}}\chi-\frac{\chi^2}{2}\right)\right]^{-1}$$

This integral does not have a closed solution, and is numerically evaluated using Gauss–Kronrod quadrature [18] by setting the absolute tolerance to 10^{-10}.

The position $\boldsymbol{x}_{\mathrm{tip}}=[x_{\mathrm{tip}}\,0\,z_{\mathrm{tip}}]^{\mathrm{T}}$ and the rotation angle $\psi_{\mathrm{tip}}=\|\boldsymbol{\psi}_{\mathrm{tip}}\|$ of the loaded end after deformation are obtained by using Howell's elliptic-integral solutions [12]:

$$x_{\mathrm{tip}}=1.408070\,\mathrm{m}$$

$$z_{\mathrm{tip}}=1.2843651\,\mathrm{m}$$

$$\psi_{\mathrm{tip}}=1.063764\,\mathrm{rad}$$

The deformed beam, as determined using Equation (14), is depicted in Figure 3. This is actually the domain $\mathscr{B}$ of inverse analysis. Then, several meshes are defined by dividing $\mathscr{B}$ into $N=2,4,8,12,16,20$ segments of equal length $h=L/N$, each one approximated using a straight finite element. The targeted solution is the undeformed beam aligned with the x-axis.

Figure 4 depicts the L_2-norm of the error in initial position $\boldsymbol{X}_0$ and rotation $\boldsymbol{\psi}$ for the different meshes. Note that a quadratic convergence rate is obtained for both error measures.

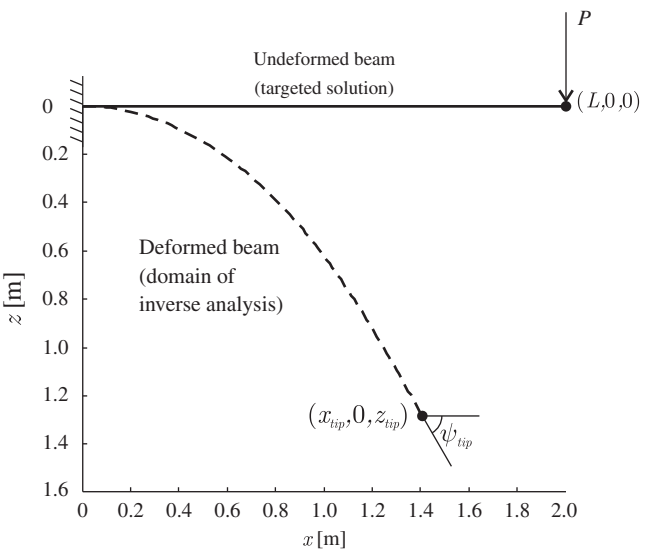

Figure 3. Plane bending of a flexible cantilever beam: undeformed and deformed neutral axes. Note that the scales for x and z are equal.

DOI: 10.1002/nme

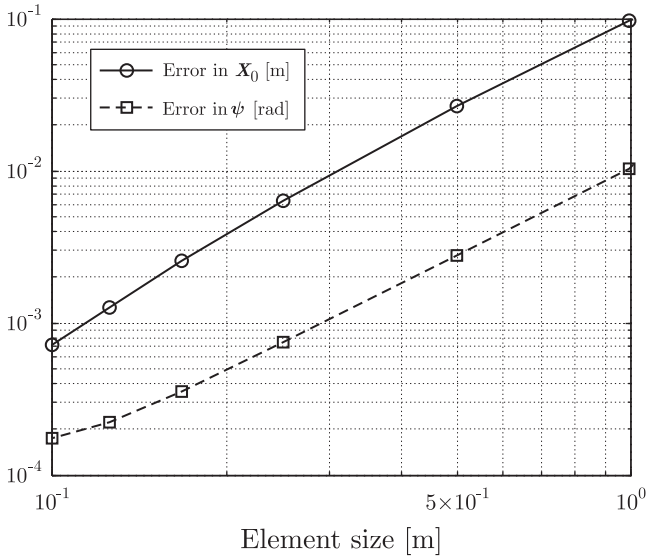

Figure 4. Bending of a flexible cantilever beam: errors in the approximation of positions and rotations (measured in L_2-norm) using the proposed inverse finite element model, as a function of the element size.

Concerning the performance of the Newton–Raphson solver, let us mention that for all the meshes considered here, it always took six iterations to attain $\|\boldsymbol{F}_{\text{int}}-\boldsymbol{F}_{\text{ext}}\|<10^{-8}\|\boldsymbol{F}_{\text{ext}}\|$ starting from the initial guess $\boldsymbol{X}_0^i=\boldsymbol{x}_0^i$ and $\boldsymbol{\psi}^i=\boldsymbol{0}$ at every node i.

5.2. *Cantilever 45-degrees bend*

Let us now consider the cantilever 45-degrees bend depicted in Figure 5. The structure is clamped at the origin O of the reference frame O-xyz, and lies in the plane xy when undeformed. The beam has a unit square cross-section, Young's modulus is $E=10^7$ and the shear modulus is $G=5\times10^6$. It is bent and twisted by the action of the force $P=600$ applied at the free end, in the z-direction. This problem was used as a benchmark for three-dimensional flexible beam models by several authors [10, 11, 13–15].

First, a direct analysis is performed. The beam is discretized using eight equal finite elements [10, 11]. The computed position of the loaded end is shown in Figure 5.

Then, an inverse analysis using the beam inverse model is performed, starting from a grid drawn on the computed deformed configuration. The solution of the inverse analysis should fit the original grid of the direct analysis. As it can be seen in Figure 5, the model is highly accurate, and almost complete agreement with the initial mesh is obtained. For instance, the distance between the given and the computed position at the free-end (loaded) node in the undeformed configuration is 0.1179 (less than 0.2% of the displacement at the same node).

A quadratic convergence rate was obtained for the Newton–Raphson iterations, taking 7 iterations to attain an equilibrium error norm $\|\boldsymbol{F}_{\text{int}}-\boldsymbol{F}_{\text{ext}}\|<10^{-8}\|\boldsymbol{F}_{\text{ext}}\|$, starting from an initial guess $\boldsymbol{X}_0^i=\boldsymbol{x}_0^i$ and $\boldsymbol{\psi}^i=\boldsymbol{0}$ at every node i.

DOI: 10.1002/nme

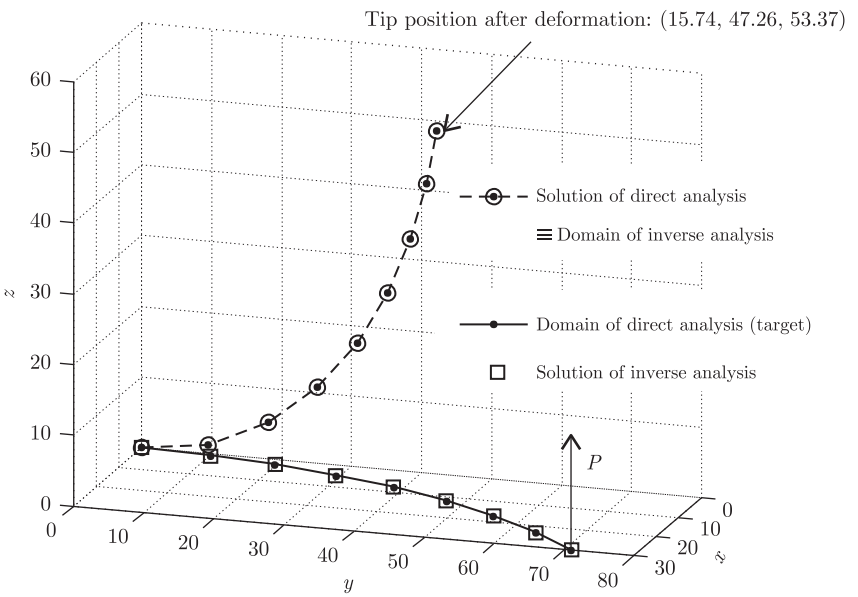

Figure 5. Cantilever 45-degree bend: solutions of direct and inverse analyses.

6. APPLICATIONS

6.1. Compliant gripper

A simple compliant gripper was proposed by Lan and Cheng [16], which allows to grab an object of a certain size and shape when acted upon. They carried out a direct analysis using intrinsic functions to parameterize the topology and the generalized multiple shooting method (GMSM) to analyze the deflection of the mechanisms. These techniques were then integrated into an optimization scheme in order to achieve the design constraints (desired shape under loading).

Figure 6 depicts the targeted loaded shape in dashed line and the actuation force $P=24\,\mathrm{N}$ applied at point C, as computed by Lan and Cheng using a quadratic polynomial to parameterize the angle of rotation of the beam axis. The gripper has constant rectangular cross-section (10 mm wide and 5 mm high), and is fixed at points A and B. It is made of polypropylene, with Young's modulus $E=1.4\times10^3\,\mathrm{N/mm^2}$ and the Poisson ratio $v=0.25$.

If we take as the domain of the analysis the desired shape of the gripper when actuated, we can apply the method of inverse analysis to compute the unknown initial shape. The deformed gripper is modeled using 46 flexible beam finite elements. The undeformed configuration obtained as solution of the current inverse analysis is depicted by a solid line in Figure 6. This solution agrees with that of Lan and Cheng, depicted by hollow circles in the same figure.

The solution of the discrete non-linear equation using the Newton–Raphson method took 6 iterations to get an equilibrium error norm $\|\boldsymbol{F}_{\mathrm{int}}-\boldsymbol{F}_{\mathrm{ext}}\|<10^{-8}\|\boldsymbol{F}_{\mathrm{ext}}\|$, starting from the initial guess $\boldsymbol{X}_0^i=\boldsymbol{x}_0^i$ and $\boldsymbol{\psi}^i=\boldsymbol{0}$ at every node i.

DOI: 10.1002/nme

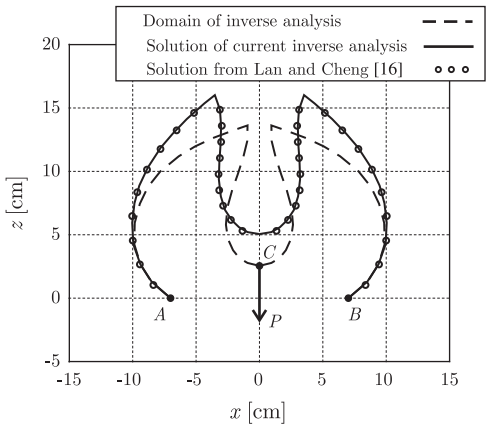

Figure 6. Compliant gripper: deformed (given design requirement) and undeformed (computed) configurations. Comparison with a reference solution [16].

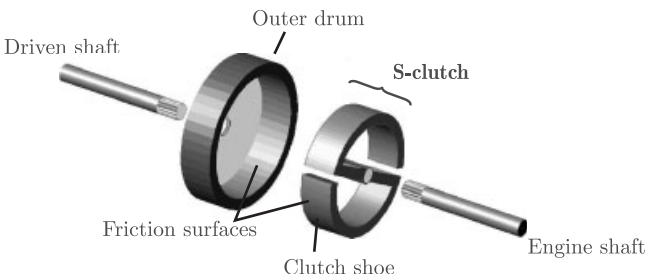

Figure 7. Compliant S-clutch.

6.2. *Compliant S-clutch*

This mechanism connects two concentric shafts (Figure 7). When deformed under the effect of centrifugal loads, the clutch shoes engage the friction surface of the outer drum. The objective is to design a clutch that engages at a certain angular speed. The deformed geometry of the clutch should match very closely the geometry of the drum to ensure a smooth distribution of the contact force between both surfaces. This reduces stress concentration and makes wear evenly distributed in the contact surfaces. Crane [19] studied this kind of mechanisms using a pseudo-rigid model. We refer to [20] for several examples of industrial S-clutches.

The S-clutch studied here is made of an aluminum alloy with $E = 69 \times 10^3\,\mathrm{N/mm^2}$ and shear modulus $G = 25 \times 10^3\,\mathrm{N/mm^2}$. In order to simplify the manufacture of the piece, the clutch shoes are assumed to have a constant rectangular cross-section (30 mm wide, 10 mm high). A second design requirement is that the clutch matches the inner diameter of the drum (110 mm) when the angular speed is 1000 RPM. Further, perfect slipping between the clutch shoes is prescribed at this speed (we could have eventually prescribe any given contact pressure as well). For the finite element inverse analysis, the desired shape was discretized using 64 equally spaced beam elements.

DOI: 10.1002/nme

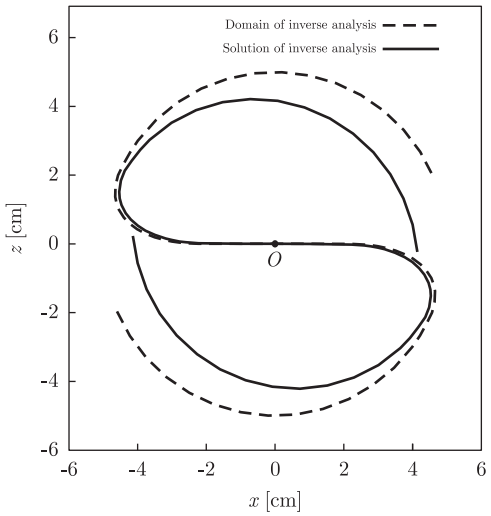

Figure 8. Compliant S-clutch: deformed (given design requirement) and undeformed (computed) configurations.

The solid line in Figure 8 represents the computed undeformed shape for manufacturing the clutch, in order to verify the design requirements. The analysis took 6 Newton–Raphson iterations to attain an equilibrium error norm $\|\boldsymbol{F}_{\text{int}} - \boldsymbol{F}_{\text{ext}}\| < 10^{-8}\|\boldsymbol{F}_{\text{ext}}\|$ starting from the initial guess $\boldsymbol{X}_0^i = \boldsymbol{x}_0^i$ and $\boldsymbol{\psi}^i = \boldsymbol{0}$ at every node i.

7. CONCLUSIONS

A finite element model for the inverse analysis of large-displacement beams has been presented. The objective in this kind of analysis is to solve inverse design problems, where the undeformed configuration is determined knowing the deformed configuration and the applied loads. A linear elastic constitutive relation is assumed.

Two- and three-dimensional test-examples have been shown, illustrating the accuracy of the model. The performance was measured either by comparison to an analytical solution (2D case) or by its ability to recover the original mesh of the corresponding direct analysis (3D case).

Two applications for compliant mechanisms design were presented. The inverse model was used for the design of a compliant gripper and a centrifugal clutch. The proposed method proved to be computationally advantageous for this kind of applications.

APPENDIX A: DERIVATIVES OF SPATIAL DEFORMATION MEASURES

Derivatives of $\boldsymbol{\gamma}$

From now on, let us obviate the subscript sp for notation convenience, keeping in mind however that all the variables are evaluated at the sampling point located at $s = L/2$.

DOI: 10.1002/nme

By taking variations in Equation (12), we obtain

$$\delta\boldsymbol{\gamma} = -\frac{1}{L}\boldsymbol{\gamma}\delta L - \frac{1}{L}\delta\boldsymbol{R}\Delta\boldsymbol{X}_0 - \frac{1}{L}\boldsymbol{R}\delta(\Delta\boldsymbol{X}_0) \tag{A1}$$

The variation of L takes the form

$$\delta L = \delta\|\Delta\boldsymbol{X}_0\| = \frac{1}{L}\Delta\boldsymbol{X}_0^{\mathrm{T}}\delta(\Delta\boldsymbol{X}_0) \tag{A2}$$

From [11], we know that

$$\delta\boldsymbol{R}\boldsymbol{u} = -\boldsymbol{R}\tilde{\boldsymbol{u}}\boldsymbol{T}\delta\boldsymbol{\psi} \tag{A3}$$

for an arbitrary vector $\boldsymbol{u}$. Then,

$$\delta\boldsymbol{R}\Delta\boldsymbol{X}_0 = -\boldsymbol{R}\widetilde{\Delta\boldsymbol{X}_0}\boldsymbol{T}\delta\boldsymbol{\psi}$$

Now, we can express the variation of $\boldsymbol{\gamma}$ given by Equation (A1) in terms of the variations $\delta\boldsymbol{\psi}$ and $\delta(\Delta\boldsymbol{X}_0)$ as follows:

$$\delta\boldsymbol{\gamma} = -\frac{1}{L}\left(\frac{1}{L}\boldsymbol{\gamma}\Delta\boldsymbol{X}_0^{\mathrm{T}} + \boldsymbol{R}\right)\delta(\Delta\boldsymbol{X}_0) + \frac{1}{L}\boldsymbol{R}\widetilde{\Delta\boldsymbol{X}_0}\boldsymbol{T}\delta\boldsymbol{\psi}$$

Since $\delta\boldsymbol{\psi} = (\delta\boldsymbol{\psi}^1 + \delta\boldsymbol{\psi}^2)/2$ and $\delta(\Delta\boldsymbol{X}_0) = \delta\boldsymbol{X}_0^2 - \delta\boldsymbol{X}_0^1$, we derive from the above equation that:

$$\frac{\partial\boldsymbol{\gamma}}{\partial\boldsymbol{X}_0^1} = \frac{1}{L}\left(\frac{1}{L}\boldsymbol{\gamma}\Delta\boldsymbol{X}_0^{\mathrm{T}} + \boldsymbol{R}\right) = -\frac{\partial\boldsymbol{\gamma}}{\partial\boldsymbol{X}_0^2}$$

$$\frac{\partial\boldsymbol{\gamma}}{\partial\boldsymbol{\psi}^1} = \frac{1}{2L}\boldsymbol{R}\widetilde{\Delta\boldsymbol{X}_0}\boldsymbol{T} = \frac{\partial\boldsymbol{\gamma}}{\partial\boldsymbol{\psi}^2}$$

Derivatives of $\boldsymbol{\kappa}$

By taking variations in Equation (13), we obtain

$$\delta\boldsymbol{\kappa} = -\frac{1}{L}\boldsymbol{\kappa}\delta L + \frac{1}{L}\delta\boldsymbol{R}\boldsymbol{T}\Delta\boldsymbol{\psi} + \frac{1}{L}\boldsymbol{R}\delta\boldsymbol{T}\Delta\boldsymbol{\psi} + \frac{1}{L}\boldsymbol{R}\boldsymbol{T}\delta(\Delta\boldsymbol{\psi}) \tag{A4}$$

Using Equation (A2), we have

$$\boldsymbol{\kappa}\delta L = \frac{1}{L}\boldsymbol{\kappa}\Delta\boldsymbol{X}_0^{\mathrm{T}}\delta(\Delta\boldsymbol{X}_0)$$

Using Equation (A3), we have

$$\delta\boldsymbol{R}\boldsymbol{T}\Delta\boldsymbol{\psi} = -\boldsymbol{R}\boldsymbol{T}\widetilde{\Delta\boldsymbol{\psi}}\boldsymbol{T}(\delta\boldsymbol{\psi})$$

In order to compute the last term in the r.h.s. of Equation (A4), note that

$$\delta\boldsymbol{T}\Delta\boldsymbol{\psi} = \boldsymbol{A}\delta\boldsymbol{\psi}$$

DOI: 10.1002/nme

with

$$\boldsymbol{A}=\left[\frac{\partial \boldsymbol{T}}{\partial \psi_1}\Delta\boldsymbol{\psi} \quad \frac{\partial \boldsymbol{T}}{\partial \psi_2}\Delta\boldsymbol{\psi} \quad \frac{\partial \boldsymbol{T}}{\partial \psi_3}\Delta\boldsymbol{\psi}\right]$$

Now, we can express the variation of $\boldsymbol{\kappa}$ given by Equation (A4) in terms of the variations $\delta\boldsymbol{\psi}$, $\delta(\Delta\boldsymbol{\psi})$ and $\delta(\Delta\boldsymbol{X}_0)$ as follows:

$$\delta\boldsymbol{\kappa}=-\frac{1}{L^2}\boldsymbol{\kappa}\Delta\boldsymbol{X}_0^{\mathrm{T}}\delta(\Delta\boldsymbol{X}_0)+\frac{1}{L}\boldsymbol{R}(\boldsymbol{A}-\boldsymbol{T}\widetilde{\Delta\boldsymbol{\psi}}\boldsymbol{T})\delta\boldsymbol{\psi}+\frac{1}{L}\boldsymbol{R}\boldsymbol{T}\delta(\Delta\boldsymbol{\psi})$$

Since $\delta\boldsymbol{\psi}=(\delta\boldsymbol{\psi}^1+\delta\boldsymbol{\psi}^2)/2$, $\delta(\Delta\boldsymbol{\psi})=\delta\boldsymbol{\psi}^2-\delta\boldsymbol{\psi}^1$ and $\delta(\Delta\boldsymbol{X}_0)=\delta\boldsymbol{X}_0^2-\delta\boldsymbol{X}_0^1$, we get from the above equation that:

$$\frac{\partial\boldsymbol{\kappa}}{\partial\boldsymbol{X}_0^1}=\frac{1}{L^2}\boldsymbol{\kappa}\Delta\boldsymbol{X}_0^{\mathrm{T}}=-\frac{\partial\boldsymbol{\kappa}}{\partial\boldsymbol{X}_0^2}$$

$$\frac{\partial\boldsymbol{\kappa}}{\partial\boldsymbol{\psi}^1}=\frac{1}{2L}\boldsymbol{R}(\boldsymbol{A}-\boldsymbol{T}\widetilde{\Delta\boldsymbol{\psi}}\boldsymbol{T}-2\boldsymbol{T})$$

$$\frac{\partial\boldsymbol{\kappa}}{\partial\boldsymbol{\psi}^2}=\frac{1}{2L}\boldsymbol{R}(\boldsymbol{A}-\boldsymbol{T}\widetilde{\Delta\boldsymbol{\psi}}\boldsymbol{T}+2\boldsymbol{T})$$

ACKNOWLEDGEMENTS

The authors gratefully acknowledge the financial support from Consejo Nacional de Investigaciones Científicas y Técnicas de la República Argentina (CONICET).

REFERENCES

1. Beck JV, Woodbury KA. Inverse problems and parameter estimation: integration of measurements and analysis. *Measurement Science and Technology* 1998; **9**:839–847.
2. Govindjee S, Mihalic PA. Computational methods for inverse finite elastostatics. *Computer Methods in Applied Mechanics and Engineering* 1996; **136**:47–57.
3. Govindjee S, Mihalic PA. Computational methods for inverse deformations in quasi-incompressible finite elasticity. *International Journal for Numerical Methods in Engineering* 1998; **43**:821–838.
4. Koishi M, Govindjee S. Inverse design methodology of a tire. *Tire Science and Technology* 2001; **29**(3):155–170.
5. Yamada T. Finite element procedure of initial shape determination for hyperelasticity. *Structural Engineering and Mechanics* 1997; **6**(2):173–183.
6. Govindjee S. Finite deformation inverse design modeling with temperature changes, axis-symmetry and anisotropy. *Technical Report UCB/SEMM-1999/01*, University of California, Berkeley, 1999.
7. Lu J, Zhou X, Raghavan ML. Computational method of inverse elastostatics for anisotropic hyperelastic solids. *International Journal for Numerical Methods in Engineering* 2007; **69**:1239–1261.
8. Fachinotti V, Cardona A, Jetteur Ph. Finite element modelling of inverse design problems in large deformations anisotropic hyperelasticity. *International Journal for Numerical Methods in Engineering* 2008; **74**:894–910.
9. Zhou X, Lu J. Inverse formulation for geometrically exact stress resultant shells. *International Journal for Numerical Methods in Engineering* 2008; **74**:1278–1302.
10. Cardona A, Géradin M. A beam finite element non-linear theory with finite rotations. *International Journal for Numerical Methods in Engineering* 1988; **26**:2403–2438.
11. Géradin M. Cardona A. *Flexible Multibody Dynamics. A Finite Element Approach*. Wiley: New York, 2000.

DOI: 10.1002/nme

12. Howell LL. *Compliant Mechanisms*. Wiley: New York, 2001.
13. Bathe K-J, Bolourchi S. Large displacement analysis of three-dimensional beam structures. *International Journal for Numerical Methods in Engineering* 1979; **14**:961–986.
14. Simo JC, Vu-Quoc L. A three-dimensional finite strain-rod model. Part II: computational aspects. *Computer Methods in Applied Mechanics and Engineering* 1986; **58**:79–116.
15. Dvorkin EN, Oñate E, Oliver J. On a non-linear formulation for curved Timoshenko elements considering large displacements/rotations increments. *International Journal for Numerical Methods in Engineering* 1988; **26**:1597–1613.
16. Lan C-C, Cheng Y-J. Distributed shape optimization of compliant mechanisms using intrinsic functions. *Proceedings of the ASME 2007 International Design Engineering Technical Conferences & Computer and Engineering Conference*, Las Vegas, NV, U.S.A., September 2007.
17. Zienkiewicz OC, Taylor RL. *The Finite Element Method*, *Volume 2*: *Solid and Structural Mechanics* (5th edn). Butterworth-Heinemann: London, 2000.
18. Shampine LF. Vectorized adaptive quadrature in Matlab. *Journal of Computational and Applied Mathematics* 2008; **211**:131–140.
19. Crane NB. Compliant centrifugal clutches: design, analysis and testing. *Master's Thesis*, Department of Mechanical Engineering, Brigham Young University, 1999.
20. Weight RG. High-torque capacity compliant centrifugal clutches. *Master's Thesis*, Department of Mechanical Engineering, Brigham Young University, 2004.

DOI: 10.1002/nme